Faculty and Researchers | Faculty and Researchers' Publications

2020-12

Evaluation of Under Sea-ice Phytoplankton Blooms in the Fully-Coupled, High-Resolution Regional Arctic System Model

Frants, Marina; Maslowski, Wieslaw; Osinski, Robert; Jeffery, Nicole; Jin, Meibing; Kinney, Jaclyn Clement

essoar.org

Evaluation of Under Sea-ice Phytoplankton Blooms in the Fully-Coupled, High-Resolution Regional Arctic System Model

Marina Frants[1], Wieslaw Maslowski[1], Robert Osinski[2], Nicole Jeffery[3], Meibing Jin[4], Jaclyn Clement Kinney[1]

[1]Naval Postgraduate School
[2]Institute of Oceanology Polish Academy of Sciences
[3]Los Alamos National Laboratories
[4]University of Alaska Fairbanks

Key Points:

- RASM reproduces the under sea-ice phytoplankton bloom observed in the Chukchi Sea in summer 2011
- Under sea-ice phytoplankton blooms are common in the Western Arctic and they occur under a specific combination of nutrient concentration and light
- High under sea-ice chlorophyll-a concentrations are also common in the Eastern Arctic, but they are at least in part a result of advection from open water blooms upstream

Corresponding author: Marina Frants, `marinarusalka@gmail.com`

Abstract

In July 2011, observations of a massive phytoplankton bloom in the ice-covered waters of the western Chukchi Sea raised questions about the extent and frequency of under sea-ice blooms and their contribution to the carbon budget in the Arctic Ocean. To address some of these questions, we use the fully-coupled, high-resolution Regional Arctic System Model to simulate Arctic marine biogeochemistry over a thirty-year period. Our results demonstrate the presence of massive under sea-ice blooms in the western Arctic not only in summer of 2011 but annually throughout the simulation period. In addition, similar blooms, yet of lower magnitude occur annually in the eastern Arctic. We investigate the constraints of nitrate concentration and photosynthetically available radiation (PAR) on the initiation, evolution and cessation of under sea-ice blooms. Our results show that increasing PAR reaching the ocean surface through the sea-ice in early summer, when the majority of ice-covered Arctic waters have sufficient surface nitrate levels, is critical to bloom initiation. However, the duration and cessation of under sea-ice blooms is controlled by available nutrient concentrations as well as by the presence of sea-ice. Since modeled critical PAR level are consistently exceeded in summer only in the western Arctic, we therefore conclude that the eastern Arctic blooms shown in our simulations did not develop under sea ice, but were instead, at least in part, formed in open waters upstream and subsequently advected by ocean currents beneath the sea ice.

Plain Language Summary

In July 2011, scientists conducting research in the western Arctic Ocean observed a large phytoplankton bloom under the sea-ice. Traditionally, such blooms were believed to be rare. Using our state-of-the-art Arctic system model, were were able to demonstrate that in fact, under sea-ice blooms have been occurring annually for the past several decades. In the western Arctic, under sea-ice blooms begin when sufficient sunlight penetrates through the sea-ice to the ocean, and end when nutrient concentrations become too low to sustain the phytoplankton. In the eastern Arctic, our model shows that under sea-ice blooms still occur even when there is not enough sunlight penetrating the sea-ice. From this, we conclude that phytoplankton blooms in the eastern Arctic begin in ice-free waters and are advected beneath the sea-ice by ocean currents.

1 Introduction

Marine phytoplankton have a strong effect on both the physical and the biological properties of the Arctic Ocean. In addition to its role in the regional carbon budget, the presence of phytoplankton alters the optical properties of sea water, affecting water temperature, mixed layer depth, upper-ocean stratification, and sea-ice cover (Manizza, Le Quere, Watson, & Buitenhuis, 2005). Phytoplankton also form the base of the marine food web, supporting a wide variety of higher trophic organisms in pelagic communities (Grebmeier, Cooper, Feder, & Sirenko, 2006; Sigler et al., 2011), while the sink of particulate organic matter produced by photosynthesis in the euphotic zone provides the main food source in benthic communities (Grebmeier & Barry, 1991).

In high-latitude environments such as the Arctic Ocean, phytoplankton growth is strongly constrained by light availability. Because light penetration into the upper ocean is attenuated by snow and sea-ice cover, it was generally believed until recently that phytoplankton growth was limited to areas of open water, with negligible growth under the sea-ice. However, under sea-ice phytoplankton blooms have been reported multiple times over the past several decades (e.g. Fortier, Fortier, Michel, and Legendre (2002); Fukuchi et al. (1989); Hill, Light, Steele, and Zimmerman (2018); Legendre, Ingram, and Poulin (1989)). In July 2011, an ICESCAPE (Impacts of Climate on EcoSystems and Chemistry of the Arctic Pacific Environment) survey observed a massive phytoplankton bloom beneath the sea ice in the northern Chukchi Sea (Arrigo et al., 2012). The phytoplank-

ton biomass was observed to be four times higher beneath the sea-ice than in the surrounding open water. The bloom extended more than 100 km beneath the pack ice with peak particulate organic carbon biomass located near the shelf break, underlying thick sea ice. The species observed indicate that pelagic diatoms were dominate, with a much smaller contribution from ice algae. The growth of this under sea-ice bloom was supported by areas of thinner first-year ice and, particularly, by the presence of melt ponds that allowed for greater penetration of light. Observational evidence suggests that this bloom was not an isolated case, and that under sea-ice blooms maybe widespread on the Arctic continental shelves (Arrigo et al., 2014; Lowry, van Dijken, & Arrigo, 2014)

The ICESCAPE observations have sparked increased interest in under sea-ice phytoplankton blooms. Several model studies have been performed to assess the physical conditions that favor the development of such blooms. Palmer et al. (2014) used a 1-D ecosystem model to demonstrate that sea-ice conditions, particularly melt pond proliferation, contributed to under sea-ice bloom formation due to the enhanced light transmission through melt pond-covered sea ice. A coupled ice-ocean model study by Zhang et al. (2015) has demonstrated a link between simulated under sea-ice blooms and increased light availability due to decreased snow cover; however, the model used in the study did not include melt ponds. Horvat et al. (2017) formulated a model based on the Sverdrup critical depth hypothesis (Sverdrup, 1953), suggesting that under sea-ice blooms can form when melt pond fraction exceeds a critical value Φ_c, but this study did not address nutrient availability, which was demonstrated to be important by Zhang et al. (2015).

The purpose of this study is to examine the temporal and spatial evolution of under sea-ice blooms in the fully-coupled, bio-physical, high-resolution Regional Arctic System Model (RASM) from 1980 to 2011. The model has been expanded to include marine biogeochemistry (mBGC) in its ocean and sea ice components, with the latter including multiple options for melt pond representation. As such, RASM is a powerful tool to investigate air-sea and bio-physical coupling in presence of sea ice at seasonal to multi-decadal time scales. We first evaluate the model bio-physical skill by comparing the modeled chlorophyll-a (chl-a) results against observations of the phytoplankton bloom in the Chukchi Sea during July 3-8 2011, as reported by Arrigo et al. (2012). Next, we examine multi-decadal variability of the under sea-ice chl-a and nutrient distributions, as well as photosynthetically available radiation (PAR) for three different decade-apart years spanning the period from 1991-2011. Finally, we discuss the relative controls of light availability and nutrient supply on the initiation and evolution of under sea-ice phytoplankton blooms in two selected regions of the western and eastern Arctic, and the contribution of these blooms to total primary production (PP).

2 The Regional Arctic System Model

RASM is a high-resolution, fully coupled atmosphere-ice-ocean-land regional model with a domain encompassing the entire marine cryosphere of the Northern Hemisphere, including the major oceanic inflow and outflow pathways, with mid-latitude extensions into the North Pacific and North Atlantic oceans to account for the passage of cyclones into the Arctic Ocean (Figure 1). The components of RASM are the Weather Research and Forecasting (WRF) model, the Variable Infiltration Capacity (VIC) land hydrology model with the river routing scheme (RVIC), and the Los Alamos National Laboratory (LANL) Parallel Ocean Program (POP) and Sea Ice (CICE) Models. The model resolution is 50 km for WRF and VIC, and 1/12° (approximately 9km) for POP and CICE. RASM has been demonstrated to correspond well with observations in its representation of the upper-ocean physical dynamics (DuVivier et al., 2016; Hamman et al., 2017; Roberts et al., 2015), arctic climate (Cassano et al., 2017; Hamman et al., 2017) and processes across the coupled atmosphere–land–ocean–sea ice interface (Brunke et al., 2018). Because this study focuses on marine biogeochemistry, only the details of POP and CICE are further described below.

2.1 Physical ocean and sea-ice model

The POP and CICE configurations used in RASM are similar to the configuration in the Community Earth System Model (CESM) version 1.1 (`http://www.cesm.ucar.edu`) however, some adjustments have been made. In addition to changes needed to use it as a regional model, POP has been modified to include a subgrid-scale brine rejection parameterization of Jin, Deal, et al. (2012); Jin, Hutchins, Kawaguchi, and Kikuchi (2012), which improves vertical ocean mixing under sea ice. Along the vertical axis, the model is configured with 45 fixed-depth layers, including 7 layers in the top 42 m. The model horizontal resolution of $1/12°$ is eddy-permitting across the entire RASM domain. The combined effects of the fully coupled model, high spatio-temporal resolution and improved parameterization of sub-grid scale bio-physical processes allowed reduction of biases in physical and mBGC model outputs when compared to the coarse-resolution CESM model (Jin et al., 2018).

The CICE model (Roberts et al., 2018) in RASM is version 6, which includes, among a number of changes, the latest column package modifications (Hunke, Lipscomb, Turner, Jeffery, & Elliot, 2015, 2016). It has been configured to include mushy-layer thermody-namics (Turner & Hunke, 2015) and Elastic Anisotropic Plastic (EAP) sea ice rheology (Wilchinsky & Feltham, 2004) , as well as the explicit level ice pond parameterization rather than the virtual melt ponds used in CESM. In addition, it uses new thermody-namic ocean coupling in which the basal freezing temperature is the same as the liquid phase temperature within sea ice. RASM CICE uses five ice thickness categories, divided at 0.65, 1.39, 2.47, 4.56 and 9.3 m.

The ice and ocean components are coupled using the coupler of Craig et al. (2012) with a coupling time step of 20 minutes to resolve sea ice-ocean inertial oscillations (Roberts et al., 2015)

The ocean and sea ice components were spun up for 78 model years, starting with the initial conditions of no sea-ice and the ocean at rest. During this stage of initializa-tion, POP and CICE models were forced with CORE2 reanalysis (Large & Yeager, 2009). Initial ocean temperature and salinity fields were from Polar science center Hydrographic Climatology (PHC 3.0), (Steele, Morley, & Ermold, 2001). After the initial stage of spin up the fully coupled version of RASM with bio-geochemical (BGC) components was run for three years starting at the first of September 1979. This three-year period was re-peated three times in order to avoid the initial shock of any component, especially the ocean and sea-ice BGC parts. The RASM production simulation, the results of which are analyzed in this paper, was started in September 1979 and continued through the end of 2018. The lateral boundary conditions at North Atlantic and Pacific sides utilized temperature and salinity information (PHC 3.0) with 30-day restoring strength. The up-per and lateral atmospheric boundary conditions for the atmospheric model were based on ERA-Interim reanalysis (Dee & Coauthors, 2011).

2.2 Marine biogeochemical model

The ocean BGC component in RASM is a medium-complexity Nutrients-Phytoplankton-Zooplankton-Detritus (NPZD) model (Moore, Doney, Kleypas, Glover, & Fung, 2002; Moore, Doney, & Lindsay, 2004; Moore, Lindsay, Doney, Long, & Misumi, 2013). The model has three phytoplankton categories: diatoms, small phytoplankton and diazotrophs, with explicit carbon, iron (Fe) and chlorophyll-a (chl-a) pools for each category, as well as an explicit Si pool for diatoms and an implicit $CaCO_3$ pool for small phytoplankton. Other state variables are: NO_3 NH_4 , Fe, Si, PO_4, a herbivorous phytoplankton pool, dissolved organic nitrogen , carbon, iron and phosphate (DON, DOC, DOFe, and DOP), oxygen, dissolved inorgranic carbon (DIC) and alkalinity.

The column package version of CICE includes two BGC parameterizations. One is a skeletal layer (SKL) parameterization in which all biological processes are assumed to be confined to a 3-cm layer at the bottom of the ice. The other is a vertical (ZBGC) parameterization in which biological activity is distributed throughout the ice column. In this study, we use the ZBGC parameterization for all our simulations. The model includes three algal categories (diatoms, small phytoplankton and *Phaeocystis sp*), two dissolved organic carbon tracers (polysaccharids and lipids), a dissolved organic nitrogen tracer, NO_3, NH_4, SiO_3, dissolved Fe (FeD), dimethylsulfide (DMS), and dissolved and particulate dimethylsulfonioproprionoate (DMSPd and DMSPp). Additional details on the sea ice BGC component can be found in Jeffery et al. (2020).

3 Conditions required for under-ice blooms

3.1 Nutrient requirements

Here we focus on nitrate as the limiting nutrient for under-ice blooms. A bloom occurs when phytoplankton growth rate exceeds the loss rate. If we assume that phytoplankton cell carbon to nitrogen ratios are fixed, then algal growth rate (G_{NO_3}) and loss rate (L_{NO_3}) are determined by nitrate uptake, and bloom permitting conditions occur when

$$L_{NO_3} = G_{NO_3} = \mu_{max}\left(\frac{NO_3}{NO_3 + \kappa_{NO_3}}\right), \tag{1}$$

where μ_{max} is the maximum algal growth rate, and κ_{NO_3}=2.5 mmol/m^3 is the half-saturation constant for nitrate uptake. The critical value of nitrate concentration necessary to produce a bloom can then be calculated as

$$NO_3 = \frac{L_{NO_3} \times \kappa_{NO_3}}{\mu_{max}\left(1 - \frac{L_{NO_3}}{\mu_{max}}\right)}. \tag{2}$$

L_{NO_3} and μ_{max} are both temperature-dependent quantities, with the temperature dependence being defined in RASM as $T_{dep} = 2.0^{((T+273.16)-(30.0+273.16))/10.0}$. Because our analysis focuses on chl-*a* in the surface layer, T is assumed to be -1.8° C as a representative surface water temperature under the ice. Thus, μ_{max} can be defined as $PC_{ref}T_{dep}$, where PC_{ref}=4.8 days^{-1} is the maximum diatom growth rate at T_{ref}=30°C and L_{NO_3} = mort×T_{dep}, where mort=0.15 day^{-1} is the diatom mortality rate. Given these assumptions, the critical nitrate concentration required to permit a bloom is NO_3=0.08 mmol/m^3.

3.2 Light requirements

When sufficient nutrients are available, the PAR becomes the limiting factor for under-ice blooms. In their model study based on the Sverdrup critical depth hypothesis (Sverdrup, 1953), Horvat et al. (2017) related PAR beneath the ice to melt ponds concentration, computing a critical melt pond fraction that would be necessary for an under-ice bloom to occur. Here we adopt a number of Horvat et al.'s assumptions, as well as their use of Sverdrup's hypothesis, to estimate the critical PAR levels necessary for an under-ice bloom. While RASM does not include PAR among its variables, it does include shortwave radiation through the ice to the ocean surface. We therefore use the 0.43 PAR to shortwave ratio estimated by Olofsson, Van Laake, and Eklundh (2007) to determine I_0, or PAR at the ocean surface under the ice. PAR at depth z can then be computed as

$$I(z) = I_0 e^{\kappa_w z}, \tag{3}$$

where $\kappa_w = 1.2$ m^{-1} is the bulk irradiance coefficient of PAR in clear water (Pegau, 2002).

Following Horvat et al. (2017), we assume a constant, depth-independent phyto-plankton decay rate Γ ($m^{-1}s^{-1}$) throughout the mixed layer. We then determine the phytoplankton growth rate as

$$G(D) = \frac{M}{D} \int_{-D}^{0} I(z)dz \qquad (4)$$

where D is the mixed layer depth, and M is a coefficient relating phytoplankton growth rate to PAR availability, so that Γ/M is the compensation irradiance. For our calculations, we used the Eastern Arctic compensation irradiance estimates of Regaudie-de-Gioux and Duarte (2010) and set $\Gamma/M = 1.3$ mol quanta m^{-2} day^{-1}, which was multiplied by a conversion factor for PAR from sunlight of 2.5 W mol^{-1} day^{-1} to give us $\Gamma/M = 3.25$ W m^{-2}.

As discussed in the section above, bloom conditions require that the phytoplankton growth rate exceeds the loss rate. We can therefore determine the critical value for I_0 by setting $G(D) = \Gamma$ and solving for I_0 to get

$$I_0 = D\kappa_w \frac{\Gamma}{M}(1 - e^{-\kappa_w D})^{-1}. \qquad (5)$$

4 Model results

Under sea-ice blooms in the Arctic are composed primarily of diatoms, both in observations (Arrigo et al., 2014) and in RASM. We therefore focus on diatoms in our evaluation of model results. All references to chl-a concentration and primary production in this paper refer specifically to diatom values. Figure 2 (a) shows modeled surface chl-a distribution in the northern Chukchi Sea during July 3-8 2011, corresponding to the dates when an under-ice bloom was detected in the region during the 2011 ICESCAPE survey (Arrigo et al. 2012). While a bloom is present in the model in the north-west corner of the region, it is located further north than the observed bloom, and the modeled chl-a concentrations are lower than the observed concentrations. Modeled ice concentrations for this time period (shown as red contours in Figure 2) indicate that the modeled sea ice has retreated further north compared to the satellite-observed sea ice conditions, and surface nitrate concentrations (not shown) are near zero throughout the region, suggesting that the model bloom has peaked earlier in the season and has consumed most available nutrients. The chl-a distribution for Jun 20-24 2011 (Figure 2 (b)), when modeled sea ice extent was similar to observed extent during the ICESCAPE cruise, shows improved correspondence to the observed bloom, with the location and spatial extent of the modeled bloom being similar to observations. However, while the maximum modeled chl-a value for the region is 21.45 mg/m^3, the observed values reach as high as 64.7 mg/m^3. Point-to-point comparison of modeled versus observed chl-a values is shown in Figure 3. The discrepancy between maximum modeled and observed values might be due to several reasons. One is the fact that that model surface atmospheric conditions, such as winds, clouds, radiative fluxes which force sea ice, are not prescribed from a reanalysis but 'predicted' from an active atmospheric model in the fully coupled configuration of RASM. Another possible reason could be the fact that the ocean model's horizontal resolution, while eddy-permitting, is not eddy-resolving and likely doesn't fully capture the mesoscale ocean dynamics, hence also small-scale local chl-a gradients that are seen in the observations. Additional discrepancies in the modeled sea ice cover might be related to inadequate coupling of horizontal momentum transfer across the atmosphere - sea ice - ocean interface.

When considering model results over a larger region of the western Arctic (Figure 4), it is clear that that the full extent of the 2011 under sea-ice bloom in the western Arctic was significantly larger than the area covered by the ICESCAPE observations. This

bloom appears annually throughout the simulation period, indicating that under-ice blooms are not a recent phenomenon. At the same time model results reveal relatively significant variability in the under sea-ice bloom distribution, magnitude and timing. To demonstrate this, Figures 4, 6 and 8 are shown with the modeled surface chl-a distributions for the western Arctic bloom (WB) region, designated as the region between latitudes 70° N and 78° N and longitudes 150° E to150° W, for the years 2011, 2001 and 1991.

In addition to the western Arctic bloom region described above, a second bloom of similar duration but of lower chl-a is simulated by the model in the eastern Arctic, and it also varies in distribution, magnitude and timing. Figures 5, 7 and 9 show the surface chl-a distributions within the eastern Arctic bloom (EB), designated as the region between latitudes 75° N and 85° N and longitudes 0° to 90° E, for the same years 2011, 2001 and 1991 as in the case of and for comparison with the WB results.

5 Discussion

To summarize the above results, the left side of Figure 10 shows the time series of spatially-integrated surface chl-a for both the EB and WB regions during May, June and July of 1991, 2001 and 2011. Previous satellite observations suggest that Arctic spring phytoplankton blooms are beginning to occur earlier in the year due to earlier sea-ice breakup and decreasing sea-ice concentrations in early summer (Kahru, Brotas, Manzano-Sarabia, & Mitchell, 2011). Our results show a similar pattern for the eastern bloom, which reached peak chl-a levels during June 19-23 in 1991, June 12-16 in 2001, and June 7-11 in 2011. However, the western bloom does not show the same pattern, with the 2001 peak (June 27-July 1) occurring later that the 1991 peak (June 22-26).

For both regions, the post-peak decline of total under sea-ice chl-a is affected by decreasing sea-ice coverage as well as by phytoplankton mortality. The EB region shows similar coverage for all three years of our analysis, with approximately 50% of the region still being covered by sea-ice by the end of July. In particular, 2001 and 2011 both show EB chl-a total decreasing from mid-June through July at a faster rate that the sea-ice coverage, indicating that the decrease is due primarily to phytoplankton loss. This loss cannot be explained by nutrient depletion, as is discussed below. By contrast, the rate of total chl-a decrease in the WB region corresponds more closely to the rate of sea-ice decrease, particularly in 2011, when under sea-ice chl-a declines to near zero at the same rate that the region becomes ice-free, suggesting that little to no actual phytoplankton loss is taking place. This is further supported by the dashed lines in the top panel of Figure 11, which show the PP for the entire WB remaining relatively constant after the under sea-ice bloom peaks.

Rows 2-4 in Figures 4 to 9 show the PAR (row 2) nutrient (row 3) and combined nutrient and PAR (row 4) conditions for the western and eastern under-ice blooms. For both regions, the period of May 15-19 in all years has been designated as "pre-bloom," while the period of July 21-25 was designated as "post-bloom." Red areas in the figures indicate the regions where nutrient and light conditions meet the critical requirements for bloom formation, as discussed in sections 3.1 and 3.2. During the pre-bloom period, nitrate concentrations are above the critical threshold throughout the ice-covered Arctic, reflecting the build-up of nutrients during the winter. As the blooms progress, nutrient concentrations become reduced, with the greater decrease occurring in the western bloom region; the eastern and central Arctic remain nutrient-replete even into the post-bloom period. Therefore, the beginning of the under sea-ice blooms is triggered by PAR availability, after which the blooms persist until the available nutrients are depleted or until the region becomes ice-free (at which point the bloom is no longer considered an under sea-ice bloom). The critical PAR criteria of Equation 5 can thus allow us to distinguish between true under-ice blooms and blooms that originally formed in open water and were subsequently advected beneath the ice. The majority of EB area in RASM

does not meet the critical PAR criteria in 2011 or 1991. However, the entire EB region still has a bloom in all three years of our study, suggesting an advective origin. This conclusion is consistent with the study of Johnsen et al. (2018), in which an under-ice bloom was observed in May 2010 northwest of Svalbard in our EB region and attributed to advection, with northward flowing water masses and southward flowing sea ice.

The advective origin of the EB is further supported by the differences in the chl-a and PP time series for the two blooms. The April chl-a totals integrated over the top 150 m for the WB (Figure 10 (a)) are near zero for all years shown. In 2011, the chl-a totals drop to zero again by August, while in 2001 and 1991 the totals drop below 5×10^7 kg but remain non-zero. This is consistent with the PP time series for the region (Figure 11 (a)), which begins near zero in April for all years and decreases to zero again in August for 2011 but not for the other two years. In contrast, the EB chl-a totals for all three years begin at approximately 1.5×10^7 kg in April and do not drop below 2×10^7 kg throughout the time series. Likewise, the PP for the EB remains non-zero for the entire time span shown in Figure 11. In fact, the full-year PP time series for the EB (not shown) indicates positive PP totals in the top 150 m starting in mid-February. The EB region does not have sufficient light to support photosynthesis that early in the year, indicating that the chl-a and PP totals must be the result of a bloom advected from an ice-free location farther south. While the maximum PP totals for the EB region are approximately half of the WB totals, the early start and long duration of the EB still make it a significant factor in the total PP for the Arctic region.

RASM simulations indicate that favorable PAR conditions for under-ice blooms have existed in the western Arctic at least as far back as 1991, allowing massive blooms to occur annually on the shelf and along the shelf break in that region. Satellite-derived estimates of sea-ice thickness have indicated that Arctic sea ice has been growing thinner since at least 1982, as multi-year ice is replaced by first-year ice (Maslanik et al., 2007). In addition, the presence and extent of melt ponds on the surface of the sea ice in the Western Arctic has been increasing over the last few decades (Hutchings & Faber, 2018). The model results suggest that if these trends continue, PAR penetration through sea-ice to the ocean surface will increase, leading to larger and earlier-occurring under sea-ice blooms, with a corresponding increase in Arctic primary production and nutrient consumption. *In situ* sampling in the EB and WB regions in the next few years would serve to confirm these results and provide a clearer picture of the effects of sea-ice reduction on Arctic Ocean biogeochemistry.

Figure Captions

Figure 1: The atmosphere/land and ice/ocean domains of the Regional Arctic System Model

Figure 2: Modeled surface chl-a distribution in the northern Chukchi Sea during July 3-8 2011 (a) and Jun 20-24 2011 (b). Circles represent the locations and observed surface chl-a concentrations for hydrographic stations sampled during the July 2011 ICESCAPE cruise (Arrigo et al., 2012). Red lines indicate modeled ice concentration; green lines in both panels indicate observed ice concentration from satellite during the ICESCAPE cruise.

Figure 3: Surface chl-a distributions for the hydrographic stations shown in Figure 2 and for the corresponding model grid cells.

Figure 4: Top row shows the modeled ocean surface chl-a distributions before, at peak chl-a, and after the Western Arctic Bloom during 2011 in the region where ice fraction is greater than 50%. Red areas in the second row indicate the regions where PAR through the ice to the ocean surface exceeds the critical value as determined in Section 3.2. Red areas in the third row indicate the regions where surface nitrate concentration exceeds the critical value as determined in Section 3.1. Red areas in the bottom row indicate the

355   regions where both PAR and nitrate exceed the their critical values. Pink contour in-
356   dicates the region of the 2011 ICESCAPE cruise (Arrigo et al., 2012)

357   Figure 5: Same as in Figure 5, but for the Eastern Arctic Bloom.

358   Figure 6: Same as in Figure 5, but for the Western Arctic Bloom in 2001.

359   Figure 7: Same as in Figure 5, but for the Eastern Arctic Bloom in 2001.

360   Figure 8: Same as in Figure 5, but for the Western Arctic Bloom in 1991.

361   Figure 9: Same as in Figure 5, but for the Eastern Arctic Bloom in 1991.

362   Figure 10: Time series of spatially integrated surface chl-a (green lines) and percentage
363   sea-ice area (black lines) for the eastern and western under sea-ice bloom areas for the
364   years 1991, 2001 and 2001. Vertical green bars delineate the 5-day period surrounding
365   the date of the chl-a maximum for each time series. Vertical gray bars delineate July 3-
366   8 2011. Dashed lines indicate the pre-bloom and post-bloom periods as shown in the first
367   and last columns of Figures 4-9

368   Figure 11: Spatially-integrated model primary production for the WB and EB regions
369   for May, June and July of 1991, 2001 and 2001. Dashed lines represent primary produc-
370   tion for the entire region. Solid lines represent primary production for the portion of the
371   region where ice concentration is greater than 50%.

## References

420   Arrigo, K. R., Perovich, D. K., Pickart, R. S., Brown, Z. W., van Djiken, G. L.,
421   Lowry, K. E., . . . Swift, J. H. (2012). Massive phytoplankton blooms under
422   Arctic sea ice. *Science*, *336*, 1408.
423   Arrigo, K. R., Perovich, D. K., Pickart, R. S., Brown, Z. W., van Djiken, G. L.,
424   Lowry, K. E., . . . Swift, J. H. (2014). Phytoplankton blooms beneath the sea
425   ice in the Chukchi sea. *Deep-Sea Res. II*, *105*, 1-16.
426   Brunke, M. A., Cassano, J. J., Dawson, N., DuVuvier, Gutowski, W. J., Hamman,
427   J., . . . Zeng, X. (2018). Evaluation of the atmosphere–land–ocean–sea ice in-
428   terface processes in the Regional Arctic System Model version 1 (RASM1)
429   using local and globally gridded observations. *Geosci. Model. Dev.*, *11*,
430   4817–4841. doi: 10.5194/gmd-11-4817-2018
431   Cassano, J., DuVivier, A., Roberts, A., Hughes, M., Seefeldt, M., Brunke, M., . . .

Zeng, X. (2017). Development of the Regional Arctic System Model (RASM): Near-surface atmosphereic climate sensitivity. . *J. Climate*, *30*, 5729-5753. doi: 10.1175/JCLI-D-15-0775.1

Dee, D. P., & Coauthors. (2011). The ERA-Interim reanalysis: configuration and performance of the data assimilation system. *Q.J.R. Meteorol. Soc.,*, *137*, 553-597. doi: 10.1002/qj.828

DuVivier, A. K., Cassano, J. J., Craig, A., Hamman, J., Maslowski, W., Nijssen, B., . . . Roberts, A. (2016). Winter Atmospheric Buoyancy Forcing and Oceanic Response during Strong Wind Events around Southeastern Greenland in the Regional Arctic System Model (RASM) for 1990–2010. *J. Climate*, *29*, 975-994. doi: 10.1175/JCLI-D-15-0592.1

Fortier, M., Fortier, L., Michel, C., & Legendre, L. (2002). Climatic and biological forcing of the vertical flux of biogenic particles under seasonal Arctic sea ice. *Mar. Ecol. Prog. Ser.*, *225*, 1-16.

Fukuchi, M., Watanabe, K., Tanimura, A., Hoshiai, T., Sasaki, H., Satoh, H., & Yamagushi, Y. (1989). A phytoplankton bloom under sea ice recorded with a moored system in LagoonSaroma Ko, Hokkaido, Japan. *Proc. Natl. Inst. Polar Res. (NIPR) Symp. Polar Biol.*, *2*, 9-15.

Grebmeier, J., & Barry, J. P. (1991). The influence of oceanographic processes on pelagic-benthic coupling in polar regions: a benthic perspective. *J. Mar. Syst.*, *2*, 495-518.

Grebmeier, J., Cooper, L. W., Feder, H. M., & Sirenko, B. I. (2006). Ecosystem dynamics of the Pacific-influenced Northern Bering and Chukchi Seas in the Amerasian Arctic. *Prog. Oceanogr.*, *71*, 331-361.

Hamman, J., Nijssen, B., Roberts, A., Craig, A., Maslowski, W., & Osinski, R. (2017). The coastal streamflow flux in the Regional Arctic System Model. *J. Geophys. Res.-Oceans*, *122*, 1683–1701. doi: 10.1002/2016JC012323

Hill, V. J., Light, B., Steele, M., & Zimmerman, R. (2018). Light availability and phytoplankton growth beneath Arctic sea ice: Integrating observations and modeling. *J. Geophys. Res.-Oceans*, *123*, 3651-3667. doi: 10.1029/2017JC013617

Horvat, C., Jones, D. R., Iams, S., Schroeder, D., Flocco, D., & Feltham, D. (2017). The frequency and extent of sub-ice phytoplankton blooms in the Arctic Ocean. *Sci. Adv.*, *3*. doi: 10.1126/sciadv.1601191

Hunke, E. C., Lipscomb, W. H., Turner, A. K., Jeffery, N., & Elliot, S. (2015). CICE: The Los Alamos sea ice model. documentation and software user's manual version 5.1 (la-cc-06-12).

Hunke, E. C., Lipscomb, W. H., Turner, A. K., Jeffery, N., & Elliot, S. (2016). CICE: The Los Alamos sea ice model. documentation and software user's manual zbgc_colpkg modifications to version 5.

Hutchings, J., & Faber, M. K. (2018). Sea-Ice Morphology Change in the Canada Basin Summer: 2006–2015 Ship Observations Compared to Observations From the 1960s to the Early 1990s. *Front. Earth Sci.*. doi: https://doi.org/10.3389/feart.2018.00123

Jeffery, N., Maltrud, M. E., Hunke, E. C., Wang, S., Wolf, J., Turner, A. K., . . . Calvin, K. (2020). Investigating controls on sea ice algal production using E3SMv1.1-BGC. *Ann. Glaciol.*, *1-22*. doi: 10.1017/aog.2020.7

Jin, M., Deal, C., Lee, S. H., Elliott, S., Hunke, E., Maltrud, M., & Jeffery, N. (2012). Investigation of Arctic sea ice and ocean primary production for the period 1992-3007 using a 3-D global ice-ocean ecosystem model. *Deep-Sea Res. II*, 28-35.

Jin, M., Deal, C., Maslowski, W., Matrai, P., Roberts, A., Osinski, R., . . . Wang, S. (2018). Effects of model resolution and ocean mixing on forced ice-ocean physical and biogeochemical simulations using global and regional system models. *J. Geophys. Res.-Oceans*, *122*. doi: 10.1002/2017JCO13365

Jin, M., Hutchins, J., Kawaguchi, Y., & Kikuchi, T. (2012). Ocean mixing with lead-dependent subgrid scale brine rejection parameterization in climate model. *J. Ocean U. China*, *11*, 473-480.

Johnsen, M., G. Norli, Moline, M., Robbins, I., von Quillfeldt, C., Sorensen, K., Cottier, F., & Berge, J. (2018). The advective origin of an under-ice spring bloom in the Arctic Ocean using multiple observational platforms. *Polar Biol.*, *41*, 1197-1216. doi: 10.1007/s00300-018-2278-5

Kahru, M., Brotas, V., Manzano-Sarabia, M., & Mitchell, B. G. (2011). Are phytoplankton blooms ocurring earlier in the arctic? *Glob. Change Biol.*. doi: 10.1111/j.1365-2486.2010.02312.x

Large, W. G., & Yeager, S. G. (2009). The global climatology of an interannually varying air-sea flux data set. *Clim. Dyn.*, *33*, 341-364.

Legendre, L., Ingram, R. G., & Poulin, M. (1989). Physical control of phytoplankton production under sea ice (Manitounuk Sound, Hudson Bay). *Can. J. Fish. Aquat. Sci.*, *38*, 1385-1392.

Lowry, K. E., van Dijken, G., & Arrigo, K. R. (2014). Evidence of under-ice phytoplankton blooms in the Chukchi Sea from 1998 to 2012. *Deep-Sea Res. II*, *105*, 105-117.

Manizza, M., Le Quere, C., Watson, A. J., & Buitenhuis, E. T. (2005). Bio-optical feedbacks among phytoplankton, upper ocean physics and sea-ice in a global model. *Geophys. Res. Lett.*, *32*. doi: 10.1029/2004GL020778

Maslanik, J. A., Fowler, C., Stroeve, J., Drobot, S., Zwally, J., Yi, D., & Emery, W. (2007). A younger, thinner Arctic ice cover: Increased potential for rapid, extensive sea-ice loss. *Geophys. Res. Lett.*, *34*. doi: 10.1029/2007GL032043

Moore, J. K., Doney, S. C., Kleypas, J. C., Glover, D. M., & Fung, I. Y. (2002). An intermediate complexity marine ecosystem model for the global domain. *Deep-Sea Res. II*, *49*, 403-462.

Moore, J. K., Doney, S. C., & Lindsay, K. (2004). Upper ocean ecosystem dynamics and iron cycling in a global three-dimensional model. *Global Biogeochem. Cy.*, *18*. doi: 10.1029/2004GB002220

Moore, J. K., Lindsay, K., Doney, S. C., Long, M. C., & Misumi, K. (2013). Marine ecosystem dynamics and biological cycling in the Community Earth System Model (CESM) [CESM1(BGC)]: Comparison of the 1990s with the 2090s under the RCP4.5 and RCP8.5 scenarios. *J Climate*, *26*, 9291-9312.

Olofsson, P., Van Laake, P. E., & Eklundh, L. (2007). Estimation of absorbed par across scandinavia from satellite measurements: Part i: Incident par. *Remote Sens Environ*, *110*, 252-261.

Pegau, W. S. (2002). Inherent optical properties of the central Arctic surface waters. *J. Geophys. Res.*, *107*.

Regaudie-de-Gioux, A., & Duarte, C. M. (2010). Compensation irradiance for planktonic community metabolism in the ocean. *Global Biogeochem Cy*, *24*. doi: 10.1029/2009GB003639

Roberts, A., Craig, A., Maslowski, W., Osinski, R., Duvivier, A., Hughes, M., . . . Brunke, M. (2015). Simulating transient ice-ocean Ekman transport in the Regional Arctic System Model and Community Earth System Model. *Ann. Glaciol.*, *56*, 211-228. doi: 10.3189/2015AoG69A760

Roberts, A., Hunke, E. C., Allard, R., Bailey, D. A., Craig, A. P., Lemieux, J. F., & Turner, M. D. (2018). Quality control for community-based sea-ice model development. *Philos. T. R.. Soc. A*, *376*, 1-18. doi: 10.1098/rsta.2017.0344

Sigler, M. F., Renner, M., Danielson, S. L., Eisner, L. B., Lauth, R. R., Kuletz, K. J., . . . Hunt, G. L. (2011). Fluxes, fins and feathers: relationships among the Bering, Chukchi and Beaufort Seas in a time of climate change. *Oceanogr.*, *24*, 251-265.

Steele, M., Morley, R., & Ermold, W. (2001). PHC: A global ocean hydrography with a high quality Arctic Ocean. *J. Climate*, *14*, 2079-2087.

542   Sverdrup, H. U. (1953). On conditions for the vernal blooming of phytoplankton. *J.*
543   *Cons. Perm. Int. Explor. Mer.*, *18*, 287-295.

544   Turner, A. K., & Hunke, E. C. (2015). Impacts of a mushy-layer thermodynamic ap-
545   proach in global sea-ice simulations using the CICE sea-ice model. *J. Geophys.*
546   *Res.-Oceans*, *120*, 1253-1275.

547   Wilchinsky, A. V., & Feltham, D. L. . (2004). A continuum anisotropic model of sea
548   ice dynamics. *P. R. Soc. London*, *460*, 2105-2140.

549   Zhang, J., Ashjian, C., Campbell, R., Spitz, Y. H., Steele, M., & Hill, V. (2015).
550   The influence of sea ice and snow cover and nutrient availability on the forma-
551   tion of massive under-ice phytoplankton blooms in the Chukchi Sea. *Deep-Sea*
552   *Res. II*, *118*, 122-135.
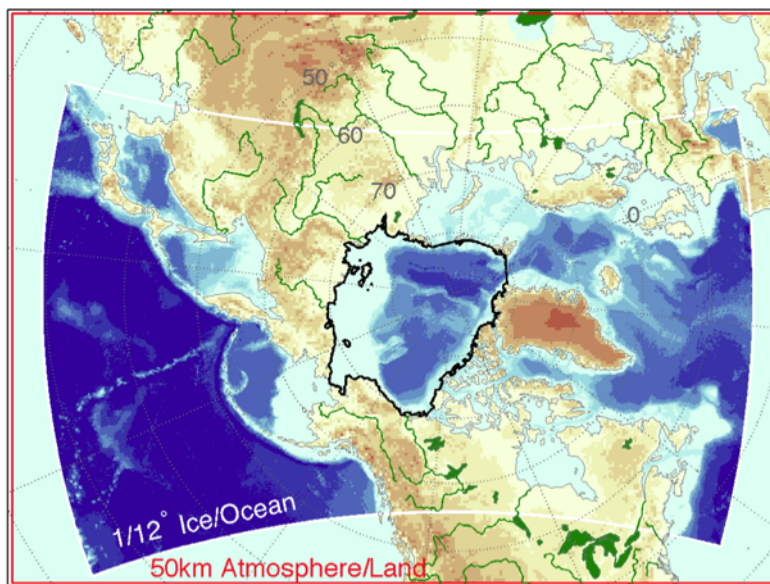
372 **Figure 1.** The atmosphere/land and ice/ocean domains of the Regional Arctic System Model
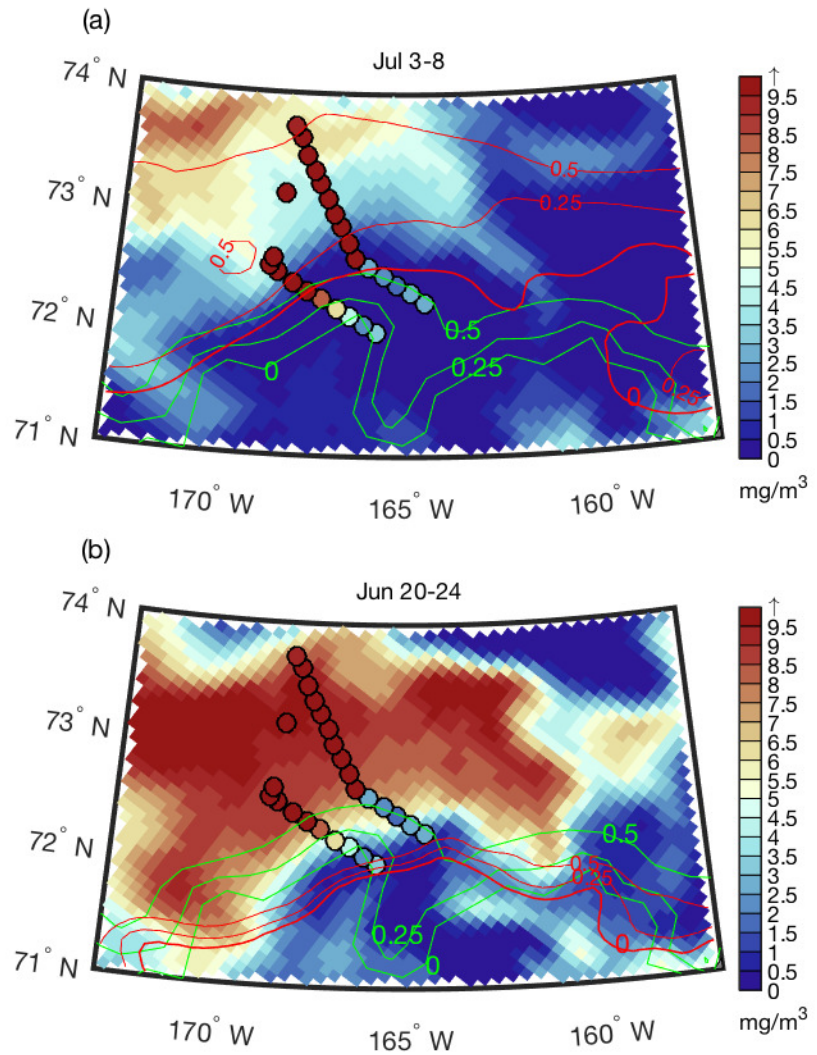
Figure 2. Modeled surface chl-*a* distribution in the northern Chukchi Sea during July 3-8 2011 (a) and Jun 20-24 2011 (b). Circles represent the locations and observed surface chl-*a* concentrations for hydrographic stations sampled during the July 2011 ICESCAPE cruise (Arrigo et al., 2012). Red lines indicate modeled ice concentration; green lines in both panels indicate observed ice concentration from satellite during the ICESCAPE cruise.
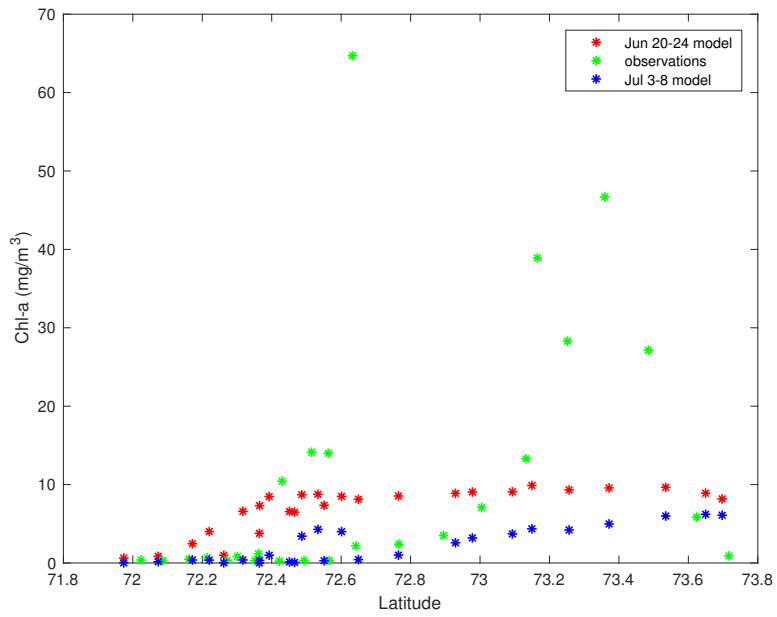
378 **Figure 3.** Surface chl-a distributions for the hydrographic stations shown in Figure 2 and for
379 the corresponding model grid cells.
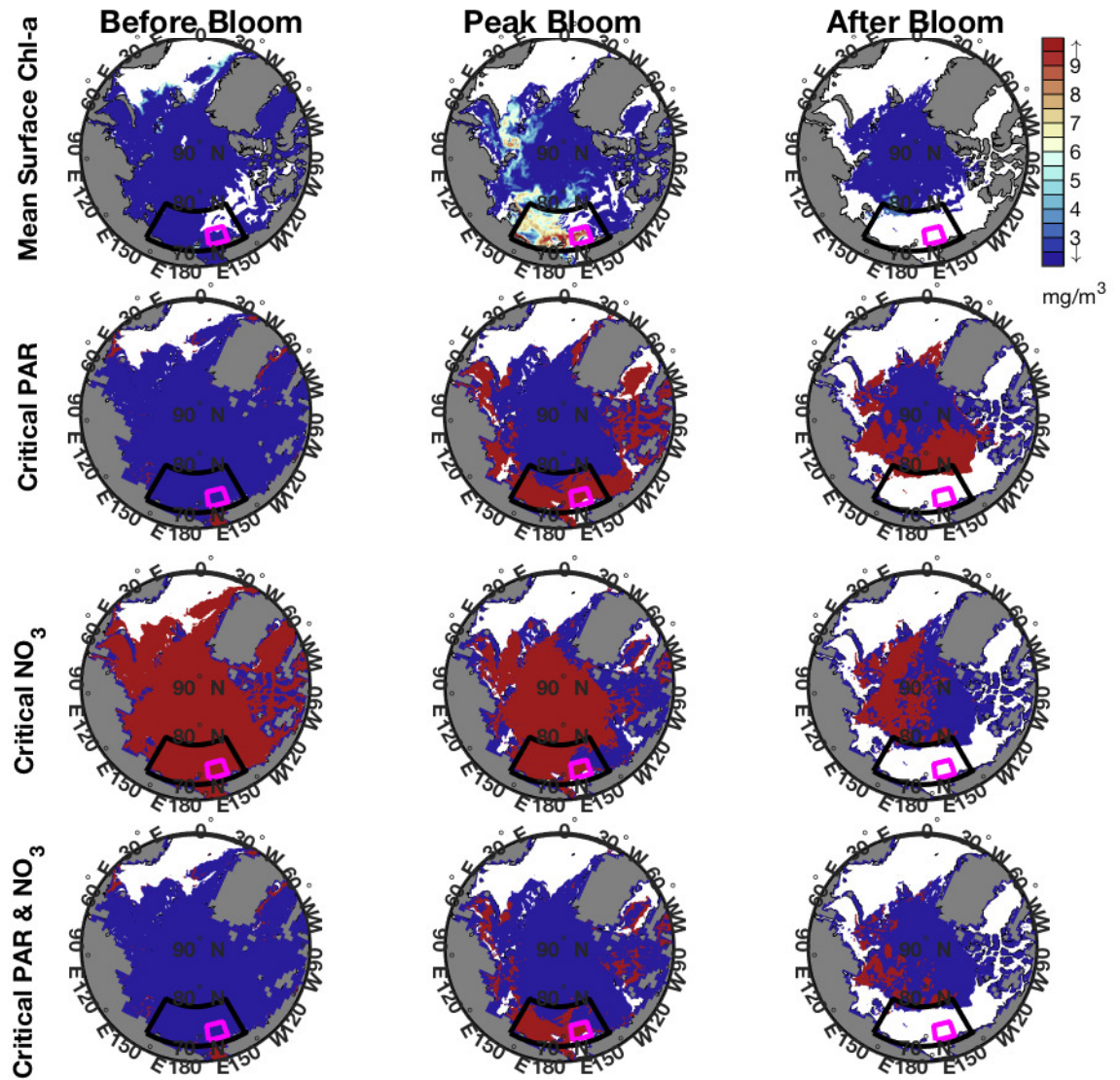
Figure 4. Top row shows the modeled ocean surface chl-a distributions before, at peak chl-a, and after the Western Arctic Bloom during 2011 in the region where ice fraction is greater than 50%. Red areas in the second row indicate the regions where PAR through the ice to the ocean surface exceeds the critical value as determined in Section 3.2. Red areas in the third row indicate the regions where surface nitrate concentration exceeds the critical value as determined in Section 3.1. Red areas in the bottom row indicate the regions where both PAR and nitrate exceed the their critical values. Pink contour indicates the region of the 2011 ICESCAPE cruise (Arrigo et al., 2012)
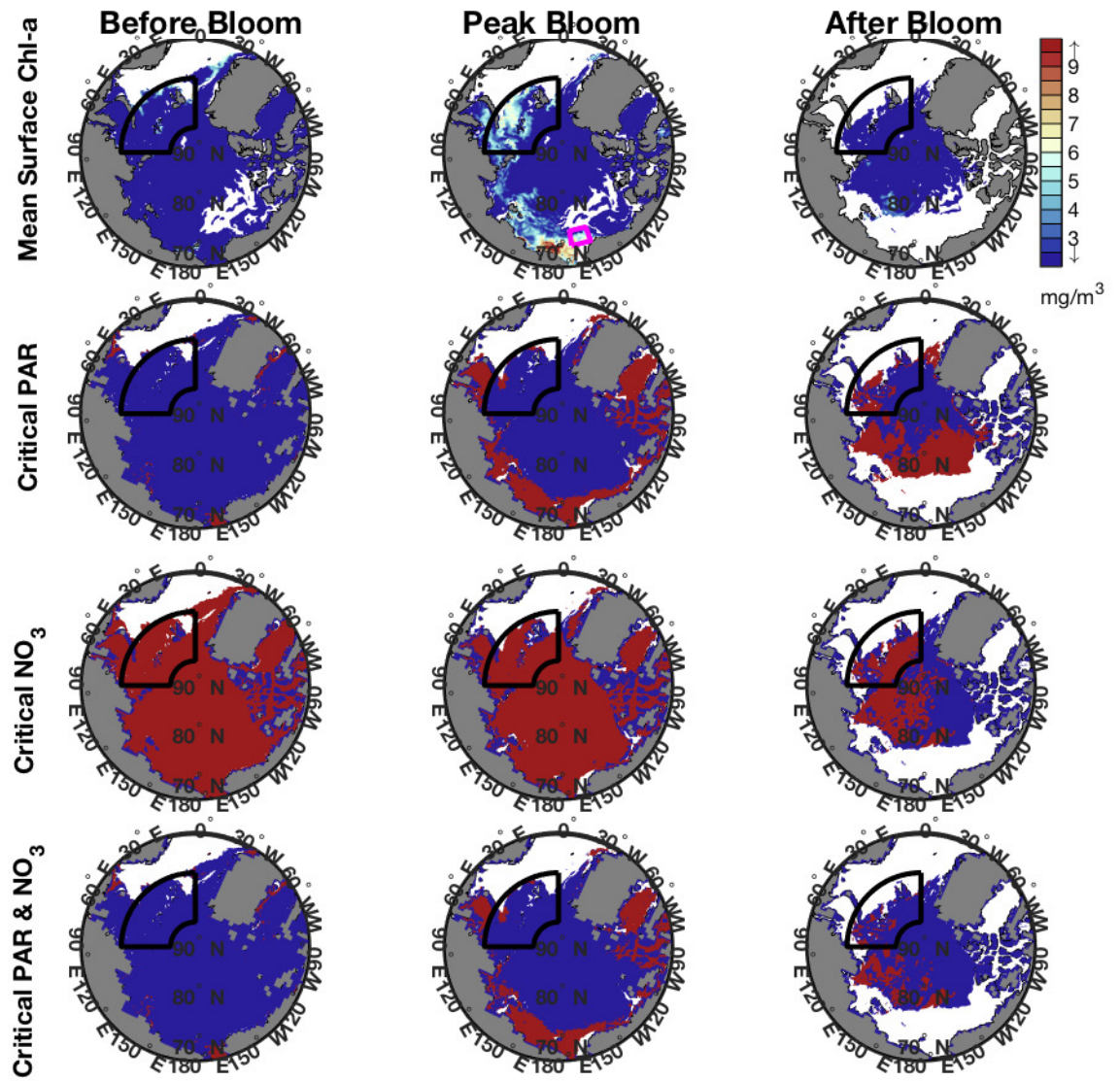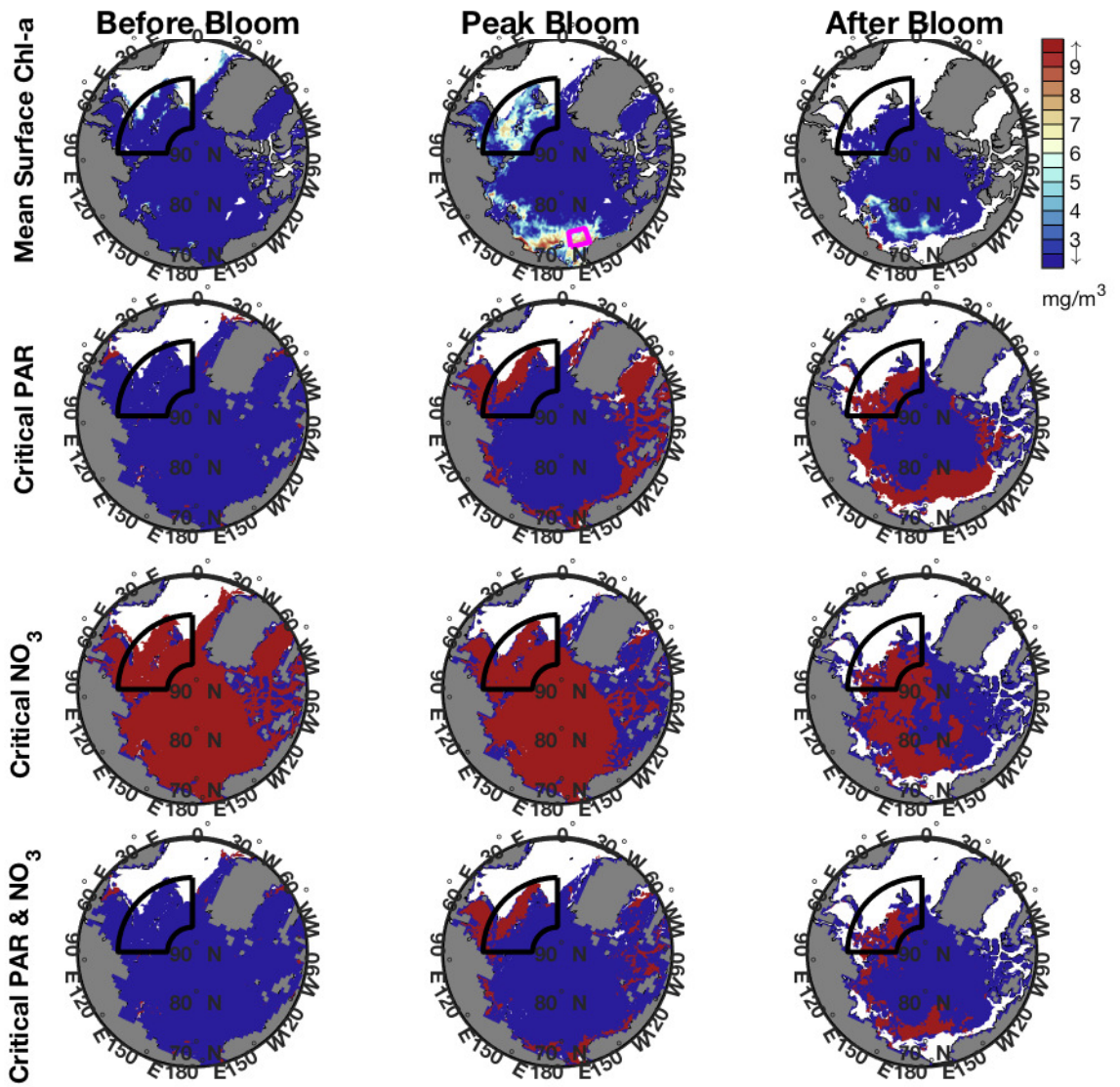
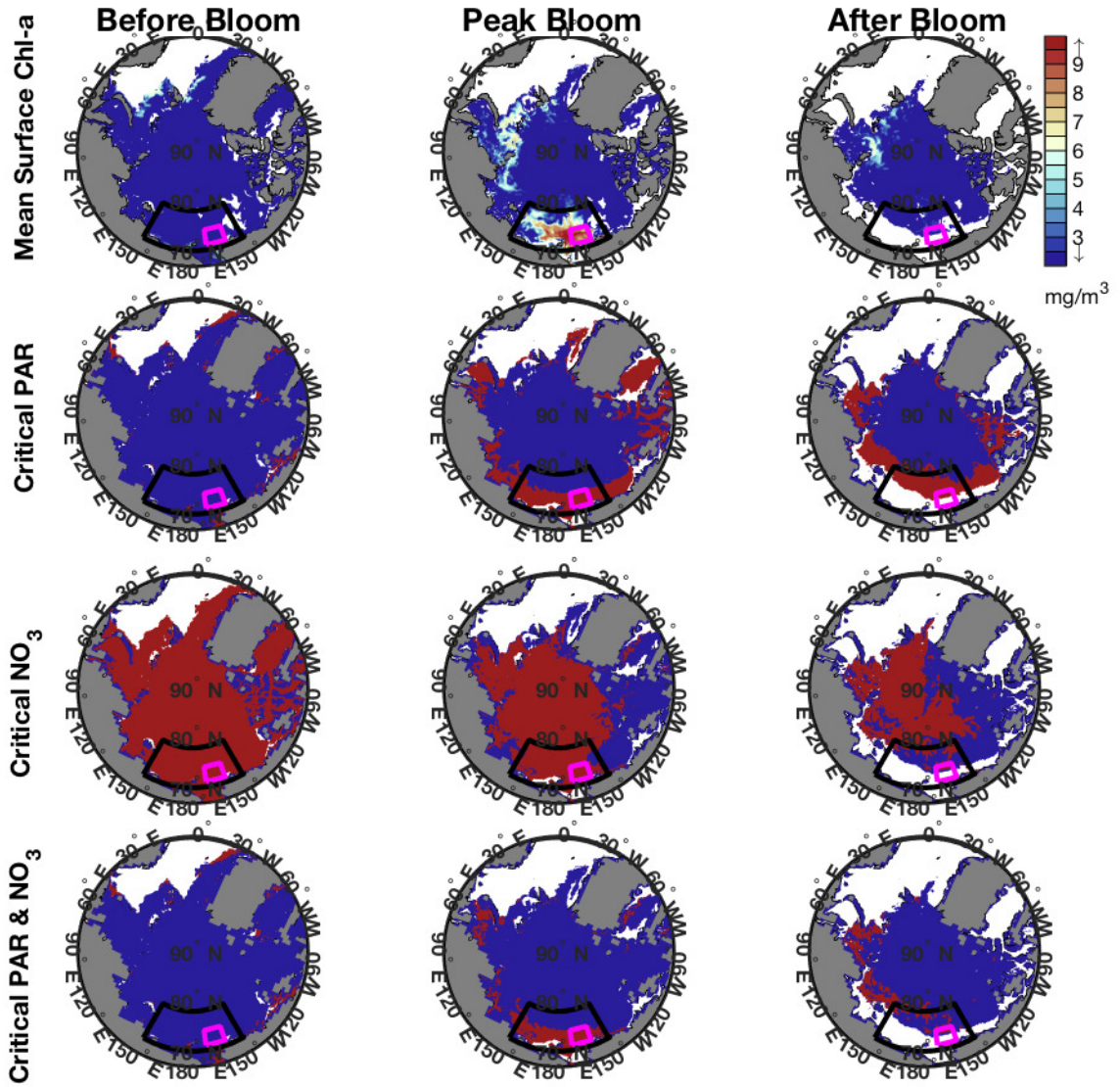**Figure 5.** Same as in Figure 5, but for the Eastern Arctic Bloom.
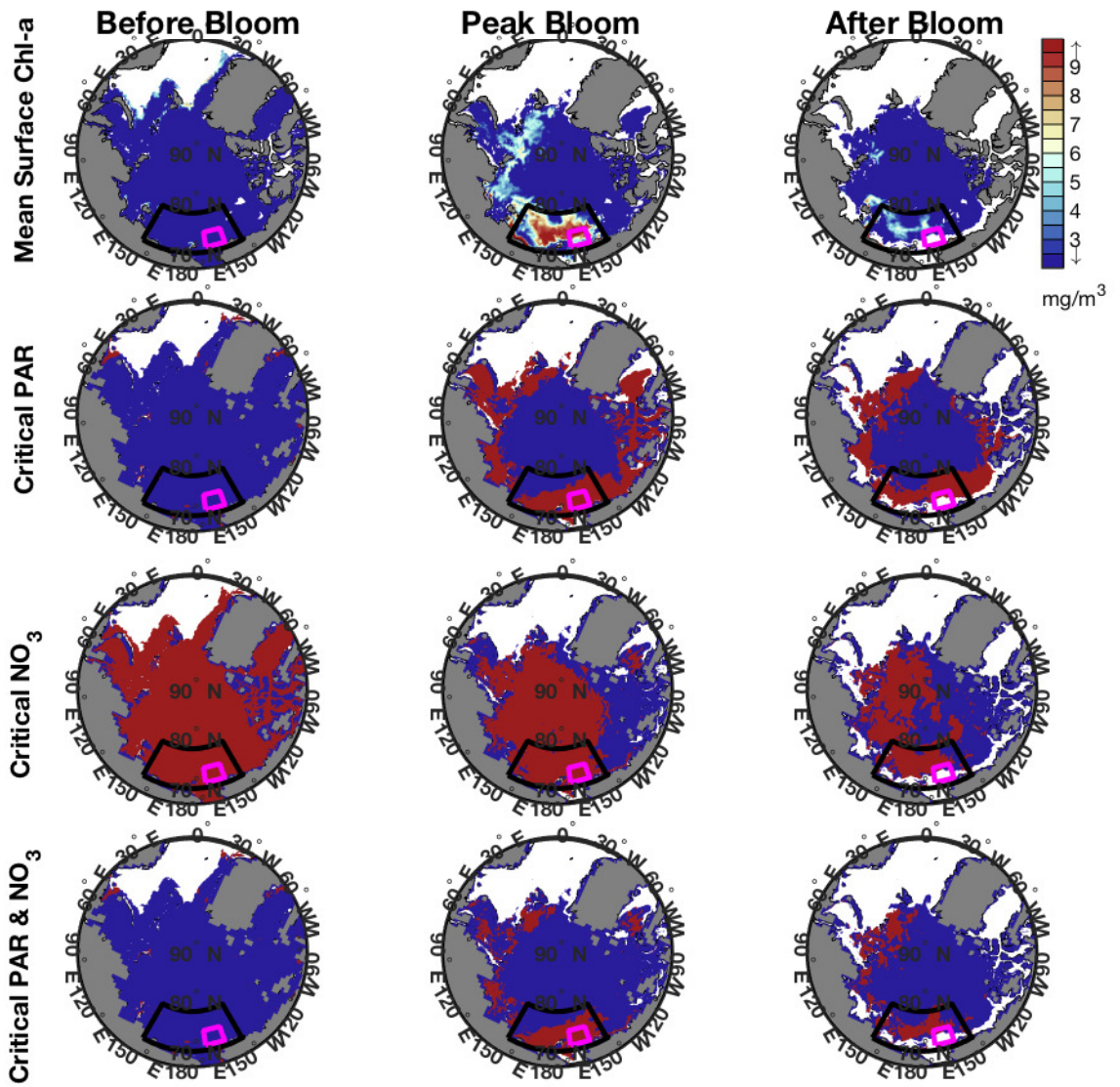
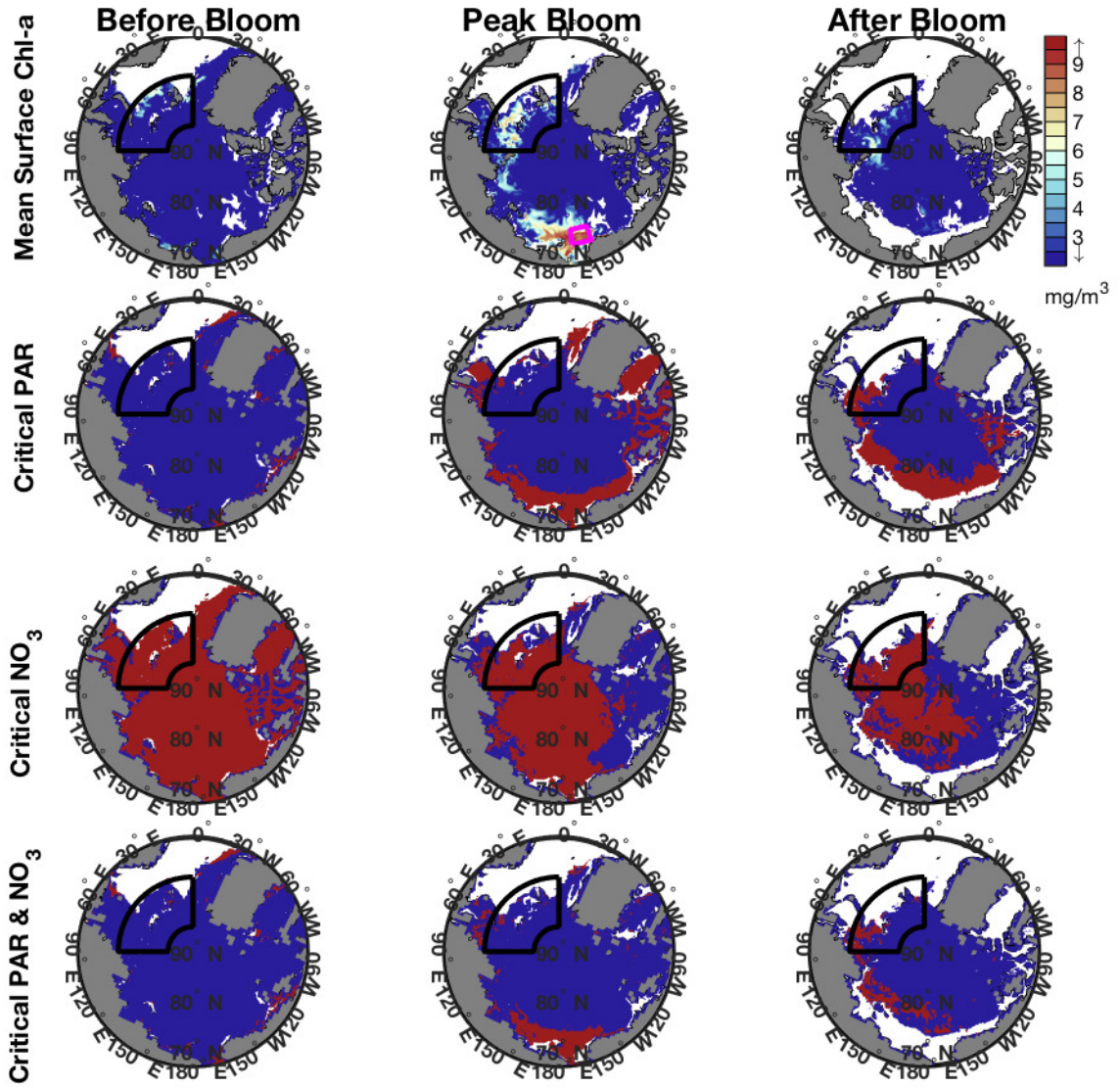**Figure 6.** Same as in Figure 4, but for the Western Arctic Bloom in 2001

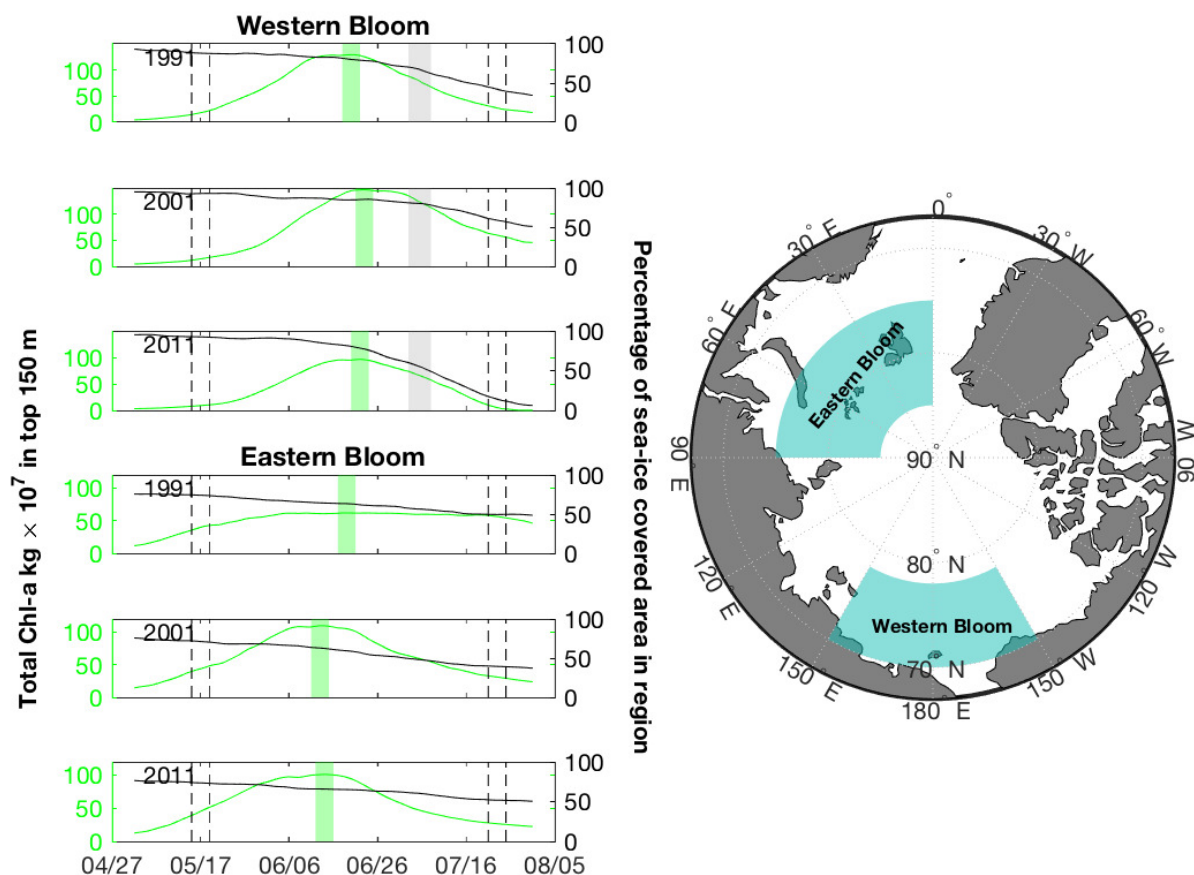**Figure 7.** Same as in Figure 4, but for the Eastern Arctic Bloom in 2001

**Figure 8.** Same as in Figure 4, but for the Western Arctic Bloom in 1991

Figure 9. Same as in Figure 4, but for the Eastern Arctic Bloom in 1991.

Figure 10. Time series of spatially integrated surface chl-a (green lines) and percentage sea-ice area (black lines) for the eastern and western under sea-ice bloom areas for the years 1991, 2001 and 2001. Vertical green bars delineate the 5-day period surrounding the date of the chl-a maximum for each time series. Vertical gray bars delineate July 3-8 2011. Dashed lines indicate the pre-bloom and post-bloom periods as shown in the first and last columns of Figures 4-9
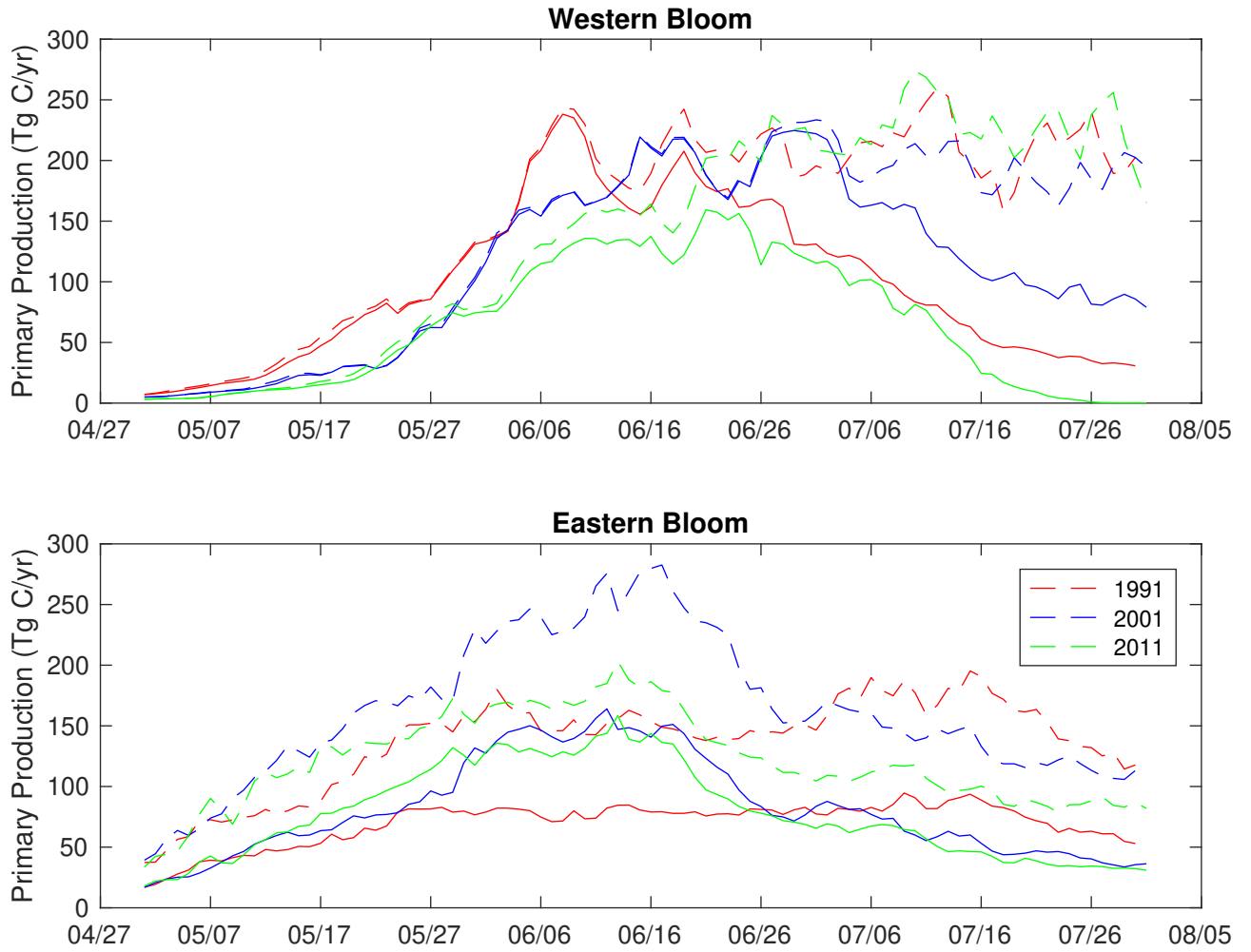
Figure 11. Spatially-integrated model primary production for the WB and EB regions for May, June and July of 1991, 2001 and 2001. Dashed lines represent primary production for the entire region. Solid lines represent primary production for the portion of the region where ice concentration is greater than 50%.